

# Topology highlights mesoscopic functional equivalence between imagery and perception: The case of hypnotizability



Esther Ibáñez-Marcelo<sup>a</sup>, Lisa Campioni<sup>b</sup>, Angkoon Phinyomark<sup>c</sup>, Giovanni Petri<sup>a,d,\*</sup>,  
Enrica L. Santarcangelo<sup>b</sup>

<sup>a</sup> ISI Foundation, Turin, Italy

<sup>b</sup> Dept. of Translational Research and New Technologies in Medicine and Surgery, University of Pisa, Pisa, Italy

<sup>c</sup> Institute of Biomedical Engineering, University of New Brunswick, Fredericton, Canada

<sup>d</sup> ISI Global Science Foundation, New York, USA

## ARTICLE INFO

### Keywords:

Hypnotizability

Imagery

Persistent homology

EEG

## ABSTRACT

The functional equivalence (FE) between imagery and perception or motion has been proposed on the basis of neuroimaging evidence of large spatially overlapping activations between real and imagined sensori-motor conditions. However, similar local activation patterns do not imply the same mesoscopic integration of brain regions, which can be described by tools from Topological Data Analysis (TDA). On the basis of behavioral findings, stronger FE has been hypothesized in the individuals with high scores of hypnotizability scores (*highs*) with respect to low hypnotizable participants (*lows*) who differ between each other in the proneness to modify memory, perception and behavior according to specific imaginative suggestions. Here we present the first EEG evidence of stronger FE in *highs*. In fact, persistent homology shows that the *highs* EEG topological asset during real and imagined sensory conditions is significantly more similar than the *lows*. As a corollary finding, persistent homology shows lower restructuring of the EEG asset in *highs* than in *lows* during both sensory and imagery tasks with respect to basal conditions. Present findings support the view that greater embodiment of mental images may be responsible for the *highs* greater proneness to respond to sensori-motor suggestions and to report involuntariness in action. In addition, findings indicate hypnotizability-related sensory and cognitive information processing and suggest that the psycho-physiological trait of hypnotizability may modulate more than one aspect of the everyday life.

## 1. Introduction

Mental imagery can be described as the ability to generate, represent and manipulate objects and events that are not physically present (de Borst and de Gelder, 2016). It has long attracted intense research as it plays an important role in human cognition, being involved in memory, abstract/spatial reasoning, action planning, decision making, skill learning and language comprehension (Kosslyn et al., 1995; Ganea and Longo, 2017). Researchers have long debated which cognitive process allows us to form perceptual/motor mental images when the corresponding sensory stimuli are absent (Kosslyn et al., 2006). The leading hypothesis, formalized by Finke (1979) and leading back to James (1890), is that a substantial *functional equivalence* (FE) exists between imagery and perception (or motion). That is, the two cognitive activities share the same neurophysiological bases, and imagery is an actual

physical simulation of perceptual and motor experience (Héту et al., 2013; Rakusa et al., 2017; Ridderinkhof and Brass, 2015). Evidence of shared mechanisms has been provided mainly by neuroimaging studies which have shown partially similar brain activations during action or perception of all sensory modalities and the correspondent mental images (Bartolomeo, 2002; Ganis et al., 2004; Ganea and Longo, 2017; Guillot et al., 2008; Kilintari et al., 2016; Halpern and Zatorre, 1999; Jeannerod, 1995; Kosslyn et al., 1995; Shin et al., 1997; Lima et al., 2015; Mizuguchi et al., 2017; Prete et al., 2016; Schmidt et al., 2014). Indeed, spatial overlap between activations provides insights into which regions perform similar roles during mental images and perception. However, local information about the spatial activation is not sufficient to conclude that the temporal activation profiles evolve similarly. In fact, while the same regions might activate in perception and mental images, their respective activation profiles might be differently correlated (Szpunar

\* Corresponding author. ISI Foundation, Turin, Italy.

E-mail address: [giovanni.petri@isi.it](mailto:giovanni.petri@isi.it) (G. Petri).

<https://doi.org/10.1016/j.neuroimage.2019.06.044>

Received 16 November 2018; Received in revised form 15 May 2019; Accepted 19 June 2019

Available online 2 July 2019

1053-8119/© 2019 Elsevier Inc. All rights reserved.

et al., 2007), and therefore activations alone are not sufficient to conclude that the brain codes in the same way for sensory information and for the correspondent mental images (Slotnick et al., 2012). A stronger marker of genuine FE should therefore lie in the coevolution of activation profiles.

### 1.1. Mental imagery and hypnotizability

Hypnotizability is a cognitive trait measured by scales (Sheehan and McConkey, 1982). It predicts the ability to accept suggestions, that is, to modify perception, memory and behaviour according to specific instructions for mental imagery (Elkins et al., 2015) (both under hypnosis and in the ordinary state of consciousness (Meyer and Lynn, 2011)), as occurs for the widely known suggestions of analgesia that allow to control pain (Hilgard and Hilgard, 2013). Different levels of hypnotizability have been associated with morphofunctional brain peculiarities (Gruzelier, 2006; Madeo et al., 2013; Landry et al., 2017), different characteristics of sensorimotor integration and cardiovascular control also in the absence of suggestions (Elkins et al., 2015), better imagery abilities in the individuals with high scores of hypnotizability (*highs*) with respect to low hypnotizable subjects (*lows*) (Scattina et al., 2012; Santarcangelo et al., 2005, 2010; Rodionov et al., 2004; Papalia et al., 2014; Carli et al., 2006). In particular, behavioral studies suggest that *highs* exhibit higher degree of FE compared to *lows* (Santarcangelo, 2014; Lebon et al., 2012; Bensafi et al., 2005; Marks and Isaac, 1995; Guillot et al., 2008; Meulen et al., 2014; Sheldon and El-Asmar, 2017). In fact, studies of the vestibulo-spinal reflex (VSR) have hypothesized stronger FE in *highs* (Santarcangelo et al., 2010) since they display the same body sway while maintaining a physically or imagined rotated position of the head. This finding is particularly relevant because the VSR, elicited by galvanic stimulation of the labyrinth, induces body sway mainly in the frontal plane when the head is directed forward and in the sagittal plane when the head is rotated toward one side (Lund and Broberg, 1983) and the VSR earlier component cannot be voluntarily modulated (Guerraz and Day, 2005; Reynolds, 2010). Interestingly, despite the reported similar vividness of the mental image of rotated head, *highs*, but not *lows*, exhibited the same VSR earlier component while maintaining the physically or imagined rotated head position. This postural finding could be sustained by stronger FE in *highs*, which could account for their greater proneness to respond to sensorimotor suggestions (that is producing ideomotor behaviors) as well as for their report of involuntariness in action. Neo-dissociative and socio-cognitive theories of hypnotic responding (Lynn and Green, 2011) interpret the subjectively reported involuntariness as an effect of the establishment of cognitive barriers between consciousness and behavior and on relational dispositions, respectively. Nonetheless, if physiological characteristics enhance the *highs* likelihood to produce ideomotor responses, then cognitive barriers should not be advocated any longer and the possible sociocognitive factors could be substituted with peculiar neurophysiological features.

### 1.2. Topological Data Analysis: persistent homology

Topological data Analysis (TDA) of the EEG is an appropriate tool to reveal hypnotizability-related brain activities configurations associated with the physically and imaginatively rotated head position which had been the object of the earliest postural investigation (Santarcangelo et al., 2010). In fact, topology (Munkres, 2000; Patania et al., 2017) describes the shape and connectivity of spaces in arbitrary dimension. Tools based on topological ideas, collectively dubbed TDA (Ghrist, 2008), emerged over the last decade to study systems where relevant scales range between different spatial and temporal resolutions, and information is encoded in higher-order interactions (Hilton and Wylie, 1967). They provide a natural language to describe local, mesoscopic and global features of data, and are therefore well-suited to capture the mesoscale organization of activation patterns. Indeed, the shape and the topological features of a dataset be it an image, a network or a matrix is effectively

described by the patterns of dense areas and the regions of disconnectivity among the former. The structure and properties of these holes define by highlighting the gaps among the denser modular parts the structure of the whole dataset. This is called the homology of the dataset, and its graded version, persistent homology, is able to deal with weighted, noisy, un-evenly sampled and complex datasets. It works by producing a sequence of progressively finer approximations called filtration of the data and by tracking the evolution of the voids across such filtration. Important features and structures in the data live longer through the filtration spanning a large range of approximations or multiple scales (for details see Methods in Section 2 and Appendix A). TDA has been recently applied to neuroimaging data to characterize resting states of consciousness: studies focused on physiological (Lord et al., 2016; Stolz et al., 2017) and altered (Petri et al., 2014; Wang et al., 2018, 2015) in resting state and during sensory tasks (Kim et al., 2015). They have also been applied to EEG data in humans to characterize cognitive tasks (Yoo et al., 2016) and in animal models to classify normal (Arai et al., 2014) and pathological behaviour (Khalid et al., 2016). Interestingly, topological features were also able to detect the encoding of geometric structure from neural activity alone in rat neuron spike data (Giusti et al., 2015; Spreemann et al., 2015), to differentiate children with attention-deficit hyperactivity disorder from autistic children using FDG-PET-based networks (Lee et al., 2012), to discriminate controls from autistic subjects based on cortical thickness data (Chung et al., 2009), and to inform the mapping between structural and functional connectomes in humans (Liang and Wang, 2017; Reimann et al., 2017; Chung et al., 2017) and animal models (Choi et al., 2014).

### 1.3. Aim of the study

The aim of the study was to find the topological correlates of sensorimotor images in comparison with the corresponding physically induced perception in *highs* and *lows*. We expected that the EEG topological difference associated with physical and imagined sensory contexts - namely the rotated position of the head- was smaller in *highs* than in *lows* (Santarcangelo et al., 2010).

## 2. Methods

Data acquisition and analysis were conducted according to the Declaration of Helsinki and approved by the local Ethics Committee. Participants signed an informed consent and their privacy was always observed.

### 2.1. Subjects

Hypnotizability was measured in a sample of 150 healthy students of the University of Pisa through the Italian version of the Stanford Scale of Hypnotic Susceptibility Scale (SSHS), form A (Weitzenhoffer and Hilgard, 1962) and classified as highly (*highs*, SHSS score  $\geq 8/12$ ), medium (mediums, SHSS score: 5 – 7/12) and low hypnotizable (*lows*, SHSS score  $\leq 4/12$ ). Among them, 20 consecutive *highs* (SHSS score (mean + SD):  $9.47 \pm 1.65$ ) and 20 consecutive *lows* (SHSS, mean + SD:  $2.01 \pm 1.89$ ) with negative anamnesis of neurological and psychiatric disease, drug free for at least the latest 2 weeks were invited to complete the Edinburgh Handedness Inventory (EHI) aimed at characterizing their handedness (Oldfield, 1971). Two *highs* and 1 Low subject were excluded because not strictly right-handed (EHI score  $< 16/18$ ); the remaining 18 *highs* (age,  $23 \pm 1.9$  yrs 11 females) and 19 *lows* (age,  $22.7 \pm 1.5$  yrs; 10 females) were invited to participate in the second part of the study consisting of EEG recording during various experimental conditions.

### 2.2. Experimental procedure

During the experimental sessions, which were conducted between 11 a.m. and 2 p.m., at least 2 h after the last meal and caffeine containing

beverage, participants were comfortably seated in a semi-reclined armchair in a sound- and light-attenuated, temperature controlled (21°C) room. The experimental procedure was entirely conducted with eyes closed and consisted of 5 trials. Each trial included a basal and a task condition lasting 1 min each. In basal conditions participants were invited to relax at their best. The tasks consisted of the visual or kinesthetic imagery of a rotated head position performed before (Time 1: v1,k1) or after (Time 2: v2,k2) maintaining an actually rotated head posture (rr). The order of the visual and kinesthetic imagery- which was the same for the trials performed before and after rr - was randomized among subjects. The scripts for the visual and kinesthetic imagery were prepared ad hoc and aimed at presenting the same mental images studied in earlier behavioral experiments (Santarcangelo et al., 2010). They were read to each participant immediately before the specific condition (v1, v2,k1,k2) and sounded as follows: for visual imagery: *Please imagine that your head is rotated towards the right side; try to see your chin aligned with your shoulder and maintain this mental image until I will tell you to stop*; for kinesthetic imagery: *Please imagine that you head is rotated towards the right side; try to feel the tension of your neck muscles and maintain this mental image until I will tell you to stop*. After each imagery task, subjects were invited to score on scales the vividness of their mental images and the experienced cognitive effort a scale from 0 (minimum) to 10 (maximum). At the end of each imagery condition they were also asked to indicate whether they had obtained better mental image of rotated head at the beginning, at the end or in the middle of the task, in order to allow to select for analysis the 20 EEG seconds in which they reported to have performed the requested task at their best. During the task of actually rotated head position, the subjects were instructed to maintain their head rotated toward the right side in order to align their chin with the right shoulder until the experimenter will allow them to change their head posture. The head position was visually controlled by one of the experimenters sitting behind the subject throughout the session.

### 2.3. EEG acquisition and processing

EEG was acquired (sample rate:1000 Hz) through a Quick-CapEEG and QuickCell<sup>®</sup> (Compumedics NeuroMedical Supplies) standard system. Thirty-two EEG electrodes were placed on the scalp according to the 10–20 International System. In addition, 2 auricular (A1, A2), 4 eye (right and left medial/lateral) and 2 EKG electrodes (standard DI lead) were placed. The electrode used as reference during acquisition was FCz; off-line the signal was referred to A1/A2 and FCz was restored. Electrodes impedance was kept under 10 kΩ. Filters were applied a posteriori (notch at 50 Hz, bandpass 0.5–45 Hz) for the signal pre-processing. The bad channels interpolated using the spherical interpolation method (EEGLAB pop\_interp function) were maximum 1 in each subject. The analysis was performed through MATLAB R2017a, EEGLab: 14.1.1b. Then, data were decomposed into source components using Independent Component Analysis (number equal to the number of electrodes, infomax ICA algorithm, EEGLAB function runica). Components were visually inspected in order to remove motion, muscular and ocular artefacts. On average, 2 ICAs were removed for each condition in each subject. The signal (total duration = 10 min) was divided into 20 s epochs (20.000 samples). The automatic selection process (deletion criteria: amplitudes > 100μV, median amplitude > 6SD of the remaining channels) removed not more than 1 epoch in each subject. For basal conditions and for the condition of really rotated head, the earliest less noisy 20 s interval (mostly between sec 0 and 30) was chosen for analysis. For the imagery tasks the selected epoch was chosen in each subject according to the interview (between sec 10 and 30 in 69% of *highs*, and 64% of *lows*).

## 2.4. Variables and statistical analysis

### 2.4.1. Subjective reports

The scores of the vividness of the mental images (range: 0–10) and of cognitive effort (range: 0–10) associated with the imagery tasks were

analyzed through repeated measures ANOVA (SPSS.15) with Hypnotizability as between subjects factor. Imagery modality (visual, kinesthetic) and Time (T1, before rr - real rotation (v1,k1); T2, after rr (v2, k2)) were within subjects factors.

### 2.4.2. EEG homological signal analysis

One of the main tools in TDA is persistent homology (PH)(Edelsbrunner and Harer, 2008; Zomorodian and Carlsson, 2005). PH captures topological data information, where topological in this context refers to arbitrary shapes in the structure of data. In particular, PH describes such shapes by quantifying the evolution of “holes” within the dataset at different scales and dimensions (0-dimensional holes correspond to the set of connected components (points), 1-dimensional holes correspond to cycles, 2-dimensional holes correspond to cavities, and so on). PH achieves this by detecting the topological features of a dataset at each scale and combining them in a robust multi-scale summary, which therefore captures –by construction– the local, mesoscopic and global properties of the data, and is robust to missing data and small errors.

PH is computed on *filtrations* of *simplicial complexes*. A simplicial complex  $X$  is a topological space described by a collection of simplices  $\sigma$ , where simplices are points, lines, triangles, and their  $n$ -dimensional counterparts (Figure B.7 in Appendix A). Simplices of dimension  $k$  are counted combinatorially by a list of  $k + 1$  vertices: a 0-simplex is a point (e.g.  $[p_0]$ ), a 1-simplex is a line (e.g.  $[p_0, p_1]$ ), a 2-simplex is a triangle (e.g.  $[p_0, p_1, p_2]$ ), and so on. To be properly defined, a simplicial complex needs to satisfy a further closure condition, that is, if  $\sigma \in X$  is a simplex in  $X$  then all the sub-simplices  $\sigma' \in \sigma$  need to belong to  $X$  too ( $\sigma' \in X$ ).

A filtration is a nested family of simplicial complexes  $\{X_i\}$  such that  $X_i \subseteq X_j$  if  $i < j$ . Filtrations are usually built in such a way as to produce progressively coarser approximations of the dataset under study. Topological features that survive along the filtration are considered relevant because they correspond to structures that live across multiple scales (Petri et al., 2013, 2014).

In this study we work with weighted graphs obtained EEG time series signals. A weighted network is a way to represent pairwise relationships and encode their strength. In our case, nodes correspond to EEG electrodes and links between nodes to the absolute value of the Pearson correlation between the nodes' signals ( $\omega_{ij} = |c_{ij}|$  for the edge between regions  $i, j$ ).

From a weighted network  $G$ , we construct the corresponding filtration of simplicial complexes as follows: i) for each edge weight  $\omega$  we build the thresholded graph  $G_\omega$  by retaining only the edges with weight larger than  $\omega$ ; ii) for each thresholded graph  $G_\omega$ , we compute the clique complex  $X_\omega$  by mapping  $k$ -cliques to  $(k-1)$ -simplices (Figure B.8); iii) by construction whenever  $\omega' < \omega$  then  $X_{\omega'} \subseteq X_\omega$ , and hence we have a filtration ordered along descending edge weights (Figure B.9).

Interestingly, although all the information is encoded in the pairwise interactions, converting a graph to a simplicial complex reveals mesoscopic organizational structure that was not appreciable at the network level, thanks to the non-locality of the topological invariants of the simplicial complex. In other words, holes in networks represent regions of altered connectivity between sets of nodes and hence topological observables encode information encoded across an intermediate number of regions/nodes and their respective connections, rather than pertaining to nodes in isolation.

Note that the possibility to consider all weight scales makes PH threshold-independent thus allowing to consider the whole correlation matrix rather than a thresholded one, as often done in the neuroimaging literature (Rubinov and Sporns, 2010). More details on persistent homology and its mathematical definition are provided in Appendix A (Ghrist, 2008).

Persistent homology can be computed to find  $n$ -dimensional holes. Here we focus on 1-dimensional holes that correspond to cycles which correspond to the generators of the homology group  $H_1$ .

The main output of PH are persistence diagrams (Fig. 1a): for each dimensionality of holes (zero-dimensional connected components, one-

dimensional loops, cavities and higher dimension analogues), a persistence diagram is a multiset of points in two dimensions, where each point corresponds to the starting point (birth step) and ending point (death step) of each hole along the filtration. Features are generally considered more important the larger their persistence is. In other words, holes that live for large intervals in the filtration capture the main features of the shape of the dataset, while shorter ones are usually considered as noise. In terms of persistence diagrams, this interpretation gives more importance to points further from the diagonal. Crucially, it is possible to compute a similarity metric between persistence diagrams, which we use to differentiate groups and conditions. We computed this similarity using the persistence scale-space kernel proposed by (Reininghaus et al., 2015) (see examples in Figure B.10 and Figure B.11). This kernel is parametrized by a scale parameter  $\sigma$  which captures how wide the Gaussian kernels on each of the points in the persistence diagrams are, and hence implicitly defines how finely or coarsely we are comparing the two persistence diagrams (Fig. 2b). Formally, given two persistence diagrams  $F$  and  $G$  (sets of birth and death cycle points), we define:

$$K_\sigma(F, G) = \frac{2K_\sigma^{\text{unnorm}}(F, G)}{K_\sigma^{\text{unnorm}}(F, F) + K_\sigma^{\text{unnorm}}(G, G)}, \quad K_\sigma \in [0, 1]$$

where,

$$K_\sigma^{\text{unnorm}}(F, G) = \frac{1}{8\pi\sigma} \sum_{p \in F, q \in G} e^{-\frac{\|p-q\|^2}{8\sigma}} - e^{-\frac{\|\widehat{p}-q\|^2}{8\sigma}},$$

$\widehat{q}$  is the mirror point of  $q$  (if  $q = (q_1, q_2)$ ,  $\widehat{q} = (q_2, q_1)$ ) and  $\sigma$  is a parameter related to the filtration step size. Note that  $K_\sigma(F, F) = 1$  for any  $F$  persistence diagram. Then, two persistence diagrams are more similar the closer their  $K_\sigma$  is to 1.

First, we compared how much the subjects' one-dimensional homological structure (i.e. the  $H_1$  group composed by cycles) changed between a task  $X$  and its corresponding basal  $bX$  ( $bX \rightarrow X$ ). For clarity, we dub this change the topological basal deviation for task  $X$ . The task and basal sets are respectively  $\{X\} = \{k1, v1, rr, k2, v2\}$  and  $\{bX\} = \{bk1, bv1, brr, bk2, bv2\}$ . For a subject  $i$  and a range of  $\sigma$  values, we computed the kernel  $K_\sigma(X^i, bX^i)$  between the 1-dimensional persistence diagrams obtained for each task  $X$  and its basal  $bX$ . We then have aggregated the similarities within a group (*highs*, *lows*) and plotted them as a function of  $\sigma$  in Fig. 1b). High similarity between two persistence diagrams corresponds to small differences in the topology of the two corresponding spaces. Furthermore, for a group of subjects, we can measure the similarity between all pairs of subjects within the group and compare it with the similarity within another group. These are the two lines in Fig. 1c).

Thus, we computed the kernel similarity  $K_\sigma(X^i, X^j)$  for task  $X$  and  $K_\sigma(bX^i, bX^j)$  for the corresponding basal  $bX$  where we consider all pair of subjects  $i, j$  in the two groups. We did not observe any specific dependence on the value of  $\sigma$ , so we can eliminate it and obtain a more compact

indicator of the difference between persistence diagrams by integrating away  $\sigma$ . Formally, for a task/basal  $a$ , group  $g$  (*highs* - H, *lows* - L) and subjects  $i, j$  belonging to  $g$ , we have considered the quantities  $\Omega_g(a, a) = \langle K_\sigma^g(a^i, a^j) \rangle_{(i,j) \in g, \sigma}$ , where the average is taken over all pairs and  $\sigma$ .

We studied the accuracy (that is the difference between imagined and real sensory context) with which imagined states reproduce the target one ( $rr$ ). We quantified the accuracy of an imaginative task  $X$  as  $\Omega(X, rr)$ . Then we ask how much imagery modifies the task patterns between *highs* and *lows*. We do this by considering the difference of accuracy between *highs* and *lows*:

$$\Delta\Omega_{HL}^{X, rr} = \Omega_H(X, rr) - \Omega_L(X, rr)$$

Positive values of  $\Delta\Omega_{HL}(X, rr)$  mean that the functional topologies of *highs* during imagery tasks and real rotations are closer than for *lows*.

Moreover, in the same way, we can also compare how imagery tasks are encoded before and after performing the actual head rotation, by considering

$$\Delta\Omega_{HL}^{X1, X2} = \Omega_H(X1, X2) - \Omega_L(X1, X2)$$

high similarity between topological features associated with physically and imaginatively rotated position of the head indicates stronger functional equivalence between imagery and perception.

Comparisons between topological observables are performed by computing confidence intervals via bootstrap resampling at 95% confidence with  $N = 10000$  replicates. In addition, for each comparison we also report standard results for t-tests on differences between groups and conditions.

### 3. Results

#### 3.1. Subjective reports

*Highs* exhibited higher vividness than *lows* (Fig. 3(left)) for both imagery modalities ( $F(1, 35) = 11.975, p < .001, \mu^2 = .255$ ). Decomposition of the significant Time  $\times$  Hypnotizability interaction ( $F(1, 35) = 11.975, p < .001, \mu^2 = .255$ ) revealed that *highs* reported the same vividness before and after the condition of actually rotated head while *lows* experienced lower vividness during later tasks with respect to the earlier ones (Time,  $F(1, 18) = 4.284, p < .053, \mu^2 = .192$ ).

*Highs* reported lower task-related cognitive effort (Fig. 3, right) than *lows* ( $F(1, 35) = 4.494, p < .041, \mu^2 = .114$ ). Decomposition of the significant Time  $\times$  Modality  $\times$  Hypnotizability interaction ( $F(1, 35) = 5.591, p < .024, \mu^2 = .138$ ) revealed that *highs* experienced lower cognitive effort during later imagery tasks independently from the imagery modality. In contrast, *lows* reported higher effort for visual imagery after the actually maintained rotation of the head than before it (Time,  $F(1, 18) = 4.788, p < .042, \mu^2 = .210$ ) and no Time difference for the kinaesthetic modality.

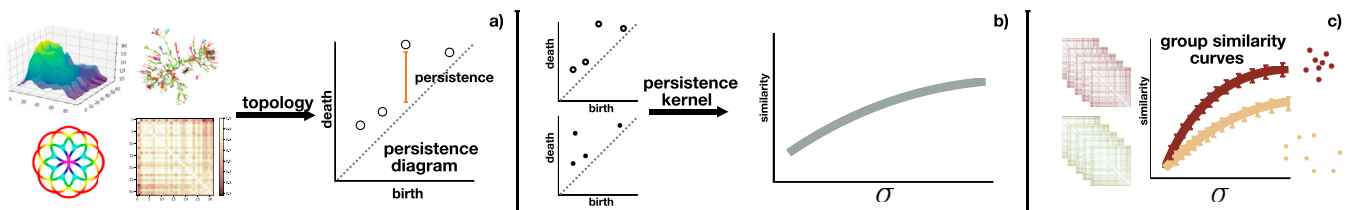


**Fig. 1. Description of the topological analysis pipeline.** a) From correlation matrix (left) to persistence diagrams (right) through persistent homology (topological features). b) Given two persistence diagrams (PDs) we define a similarity measure between them.  $\sigma$  is a parameter of the kernel which encodes the resolution at which we compare the persistence diagrams; larger  $\sigma$  values correspond to a coarser comparison on the respective positions of the points of the persistence diagrams being compared. c) Similarity measure applied on a set of PDs for two different groups.

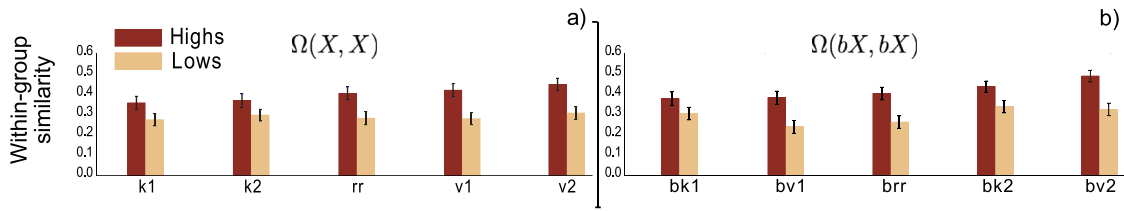


**Fig. 2. Higher homogeneity in *highs* group respect to *lows* both in basal and task condition.** Confidence intervals have been computed via bootstrap of the mean at 95% confidence level. We bootstrap within-group similarity values (bootstrap samples = 10000) and compute mean with its corresponding confidence interval. All group average comparisons are significantly different. For statistics see [Appendix B, Table B.1](#).

### 3.2. Topological Data Analysis

a) **Intra-group topological homogeneity.** According to the  $\Omega$  values obtained for intragroup similarities (Fig. 2), *highs* report higher values of  $\Omega$  for all basal and task conditions (bootstrapped confidence intervals at 95% confidence level, samples  $N = 10000$ , and  $t$ -test  $p \ll 0.001$ ,  $t \in \{4, 10\}$ ), implying that the *highs* are more similar to each other than *lows* are in all task and basal conditions.

b) **Deviation from basal conditions during tasks.** As shown in Fig. 4, the *highs* topological similarity between tasks and basal conditions was significantly greater than the *lows*' (bootstrapped confidence intervals at 95% confidence level, samples  $N = 10000$ , and statistics for  $t$ -tests reported in [Appendix B Table B.2](#)). This indicates that the *highs* imaginative and sensorimotor tasks required less topological restructuring with respect to *lows*.

Although subjective experience can rarely be reconduced to a single physiological index (Cheron et al., 2016), it is noticeable that the degree of topological restructuring was negatively correlated with the cognitive effort reported for imagery tasks. We quantify this using the Spearman rank correlation (Spearman, 1904), which measures the correlation between orderings of elements, rather than their linear dependence, and hence allows for any monotonous relationship between the compared data (Spearman  $R = -0.3$ ,  $p < 0.05$ , [Figure B.12](#)).

c) **Differences between real and imagined sensory conditions.** The functional topologies of *highs* during imagery tasks and real rotation were closer to each other than in the case of the *lows*; (Fig. 5a), as indicated by the higher similarity between the two conditions observed in *highs*. In the comparison between the imagery tasks preceding and following the real head rotation through the value of  $\Delta\Omega_{HL}^{X1, X2}$ , we found that *highs* again display smaller distances between the encoding of the respective imaginations (v1/v2, k1/k2) before and after the real rotation (Fig. 5b)). All confidence intervals were calculated via bootstrap at 95% confidence level, samples  $N = 10000$ . Further statistical results are reported [Appendix B Table B.3](#).

d) **Learning effects.** In order to compare basal deviation of the real rotation with that of the imagined ones we computed the difference:

$$\Xi_g^{rr, X} = \left| \Omega_g(rr, brr) - \Omega_g(X, bX) \right|,$$

for a group  $g$ .

In Fig. 6 we show the results for all imagery task. The difference reported point toward a substantial decrease of  $\Delta\Xi_g^{rr, X}$  in *highs* after the real rotation and an increase in *lows* for both imaginations. In other words, we showed that basal deviation, is closely associated with cognitive effort, with *highs* displaying small deviations, in fact a decrease, and more uniformity topological structure as compared to *lows* (bootstrapped confidence intervals at 95% confidence level, samples  $N = 10000$ , results for  $T$ -tests on group averages in [Appendix B; Table B.4](#)).

## 4. Discussion

Findings show that topological properties describe hypnotizability-related differences in FE between imagery and perception and, more broadly, in sensori-cognitive-information processing. In fact, we report here the first evidence of stronger functional equivalence in *highs* who display smaller differences between the physically and imaginatively rotated head position with respect to *lows* (Fig. 5), supporting the hypotheses of stronger FE in *highs* raised from behavioral studies (Santarcangelo et al., 2010). Crucially, the reported differences being topological in nature stem from changes in the overall structure of brain activation patterns, rather than from localized or region-specific changes. Hypnotizability-related differences have been observed also in learning as *highs* reduced their cognitive restructuring during the imaginative tasks performed after the real rotation, while *lows* increased it. Since *highs* reported the same vividness for earlier and later tasks, this suggests that *highs* improve their imaginative performance by obtaining the same vividness through lower restructuring, whereas *lows* obtain lower vividness of visual imagery despite greater restructuring. It is possible that *lows* did not report decrease vividness of the kinesthetic image because the recently experienced physical rotation of the head primed the cognitive task (Anuar et al., 2017). Our results based on the similarity in the co-activation shapes across different EEG signals (rather than of spatial similarity of regional activations) are in line with previous

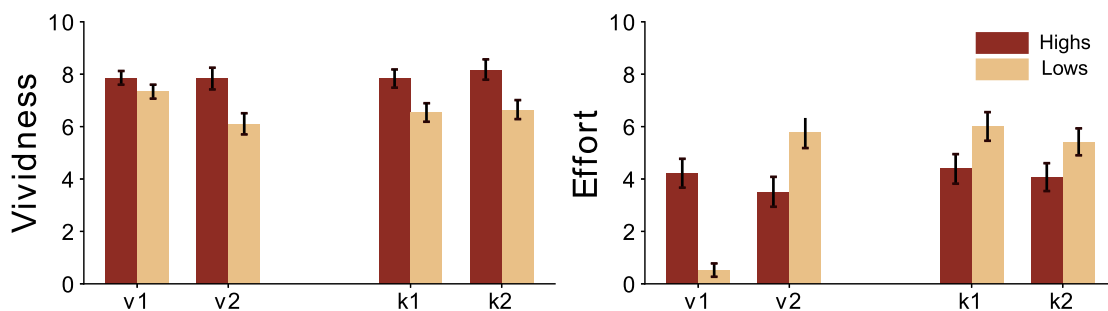


**Fig. 3. Subjective reports.** (Mean, SEM) of vividness of imagery (left panel) and cognitive effort (right panel). *highs* reported significantly higher vividness and lower effort than *lows*. *Lows* reported lower vividness for later tasks. The *highs*' effort was greater for earlier than for later tasks. v1/k1 and v2/k2: visual and kinesthetic imagery before/after the actually rotated position of the head, respectively. For statistics, see text.

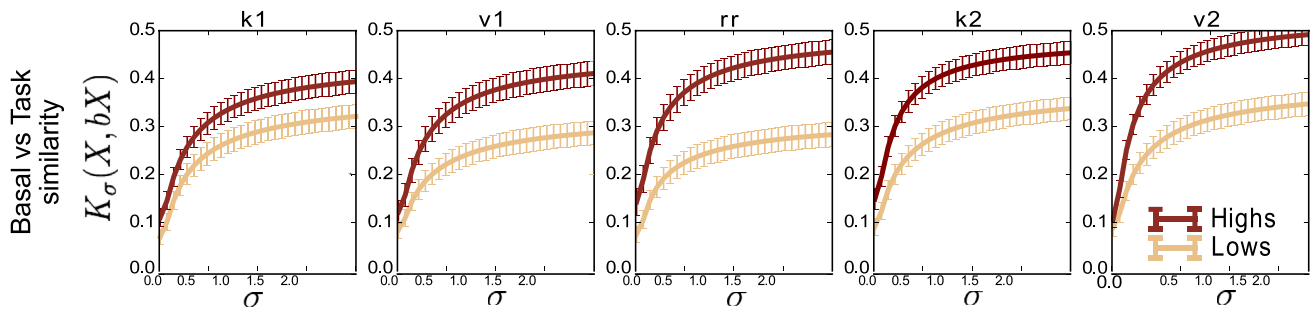


**Fig. 4.** Comparison of similarity between *highs* and *lows* for all basal-task pairs  $bX \rightarrow X$ . The basal deviation of *highs* is always smaller ( $K_\sigma(X, bX)$  is higher) than in *lows*. Confidence intervals have been computed via bootstrap of the mean at 95% confidence level. We bootstrap basal vs task similarity values (bootstrap samples = 10000) and compute mean with its corresponding confidence interval. For additional statistical results, see [Appendix B, Table B.2](#).

evidence indicating greater imagery abilities in *highs* (Carli et al., 2007) (Santarcangelo et al., 2010) (Scattina et al., 2012).

#### 4.1. Functional equivalence between imagery and perception

The stronger FE between imagery and perception observed in *highs* may provide significant advancement in the physiology of the response to suggestions. In fact, theoretically a better simulation of physically induced perception may facilitate the response to sensori-motor suggestions and possibly account for the involuntariness in action reported by the *highs* experiencing the subjective and behavioral effects of sensori-motor suggestions (Santarcangelo, 2014). The perception of involuntariness in action is a main component of hypnotic responding and has been differently interpreted (Ruehle and Zamansky, 1997) by the neo-dissociative (Hilgard, 1991; Bowers, 1992) and socio-cognitive (Lynn, 1997; Spanos, 1986) theories of hypnosis. The former assume that hypnotic responding is reported as involuntary for the dissociation between behavior and conscious experience, which could be likely accounted for by the observed modulation of the functional connection between the salience and executive circuits in *highs* (Landry et al., 2017). In contrast, socio-cognitive theories propose that the experience of involuntariness may be sustained by peculiar configurations of cognitive, emotional, relational and sociocultural traits which make the suggested perception/behavior the most adequate to a given situation, so that it is triggered automatically and experienced as effortless and involuntary (Lynn, 1997; Lynn and Green, 2011). We think that, at least for sensori-motor suggestions, stronger FE between imagery and perception

can support the greater proneness to ideomotor behavior and the relative experience of low effort and involuntariness (Santarcangelo, 2014). In clinical contexts, the strength of the functional equivalence between imagery and perception may predict the efficacy of imaginative training in neuro-rehabilitation (Caligiore et al., 2017; Tong et al., 2017) and sports (Ridderinkhof and Brass, 2015; Frank and Schack, 2017). In this respect, hypnotic assessment could become an easy and cheap tool to orient the set-up of individualized mental training.

#### 4.2. Sensory-cognitive information processing

We hypothesize that the scarce topological changes occurring in *highs* during tasks with respect to basal conditions are the effect of largely distributed information processing. This is in line with the observation of greater homogeneity within *highs* and with the findings of spectral analysis revealing more widespread desynchronization in *highs* than in *lows* during both visual and somesthetic imagery (Cavallaro et al., 2010). The scarce changes observed in *highs* agree with the findings of Recurrence Quantification Analysis which failed to detect differences in the EEG Recurrence Plot of *highs* when they did and did not receive efficacious suggestions of analgesia during nociceptive stimulation (Madedo et al., 2015). Although the performance at cognitive and motor tasks has been associated with reconfiguration of the brain functional connectivity (Elton and Gao, 2015; Schultz and Cole, 2016), higher intelligence has been found associated with scarce task-related brain network reconfiguration (Schultz and Cole, 2016) and spectral analysis supports the view that the lower the power changes the higher the cognitive performance

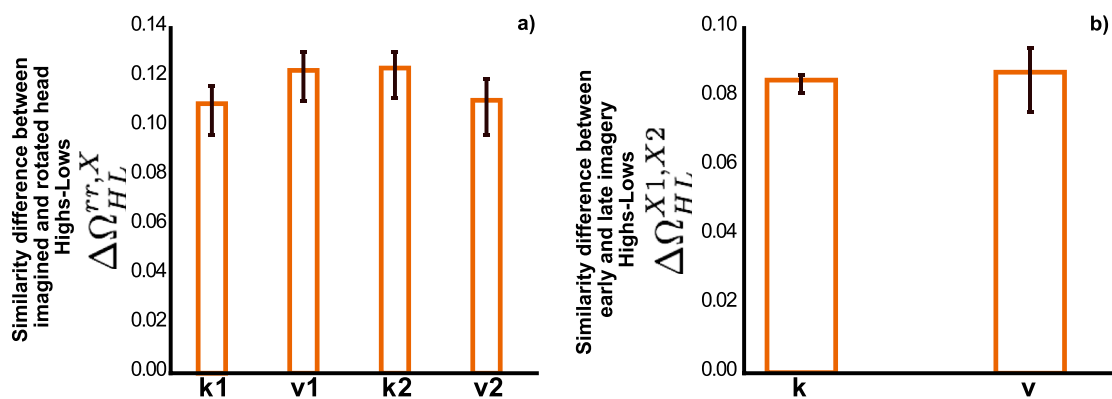


**Fig. 5.** Similarity difference between imagined and actual position of rotated head. a) Difference between *highs* and *lows* in imagery tasks as compared to actual head rotations. Positive values indicate that *highs* are topologically nearer to the real rotation than *lows*. Error bars correspond to 95% confidence level on the mean. b) Difference between *highs* and *lows* of the alteration of topology between tasks before and after rotation (v1 vs v2, k1 vs k2). Positive results mean that *highs* display more similar topologies before and after the rotation, as compared to *lows*. a) & b) Note that  $\Delta\Omega$  is related to the area between the two similarity curves that are being compared. Confidence intervals have been computed using the bootstrapping technique on the subsampled averaged on a 95% level. We bootstrap  $\Delta\Omega_{HL}^{r,X}$  (left figure) and  $\Delta\Omega_{HL}^{X1,X2}$  (right figure) values (bootstrap samples = 10000) and compute mean with its corresponding confidence interval. For additional statistics, see [Appendix B, Table B.3](#).

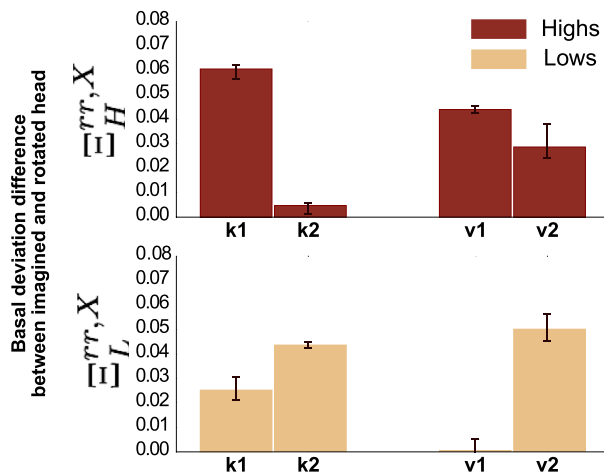


**Fig. 6. Imagery induced alteration of topology compared to rotation induced changes.** We quantify using  $\Xi_{g}^{r,X}$  the change in effort before and after the real rotation, which can be related to task adaptation. Highs display a decrease of the difference between basal deviation between real and imagery-task, while lows show a clear increase. This is associated with the decreased effort experienced by highs and the increased effort experienced by lows during later imagery tasks. Confidence intervals have been computed via bootstrap of the mean at 95% confidence level. We bootstrap  $\Xi_{HL}^{r,X}$  (left figure) and  $\Xi_{HL}^{X1,X2}$  (right figure) values (bootstrap samples = 10000) and compute mean with its corresponding confidence interval. For additional statistical results, see Appendix B, Table B.4.

(Smith et al., 1999; Hatfield et al., 2004; Del Percio et al., 2010; Cheron et al., 2016). Indeed, we have sufficient evidence for the highs extraordinary ability to perform cognitive tasks. It is indicated by their peculiar attentional ability (Crawford, 1994; Cojan et al., 2015), their proneness to disregard irrelevant information (David and Brown, 2002), to voluntarily modulate their conscious experience according to specific suggestions (Meyer and Lynn, 2011) and to modify their state of consciousness voluntarily (Pekala et al., 2017).

It has been proposed that the mechanisms underlying cognitive activities change activation patterns characterized by a more segregated, within network structure into other patterns characterized by pre-eminent between networks connectivity (Sporns, 2013). The shift from one to the other could be induced by ascending neuro-modulatory systems (Shine et al., 2016; Bell and Shine, 2016). The latter might be more efficient in highs and maintain their EEG activity in a highly distributed mode of functioning independently from tasks. In highs, in fact, we have indirect evidence of hyperactivity of the cholinergic and/or noradrenergic system indicated by their shorter reaction times in attentional tasks (Castellani et al., 2007; Castellani and Sebastiani, 2008) and of higher dopaminergic tone (Di Gruttola et al., 2014). In addition, findings of hypnotizability-related morpho-functional cerebellar differences (Picerni et al., 2018; Bocci et al., 0000; Menzocchi et al., 2015) allow to hypothesize a reduced cerebellar inhibition of the cerebral cortex.

#### 4.3. Limitations

Although imagery is bilaterally represented in the brain (Cremades and Pease, 2007), the actual position of head rotated toward the right side may have activated the left and right hemisphere differentially. Thus, a limitation of the study is that the EEG laterality was not taken into account. It would have increased the number of factors of variability too much with respect to the sample size. Indeed, a much larger sample would also allow for a more sophisticated hypnotic assessment able to differentiate highs and their topological features according to their

hypnotic profile (that is the quality of the items they passed on the scoring scale) rather than simply to the total score reported on hypnotizability scales (Terhune and Cardeña, 2015). Present findings allow to suggest that the highs response to sensory suggestions could be facilitated by larger superimposition of the cortical activations associated with imagined and physically induced sensory experience, thus sustaining the reported involuntariness in action. Nonetheless, this mechanism may be not sufficient to explain the effects of suggestions in different domains such as distortion/suppression of memories and perception. The latter could be better accounted for by relational dispositions whose biological substrates are now coming to evidence (Kirsch, 2018; Kasos et al., 2018).

#### 4.4. Conclusions

Topological properties provide the first evidence of EEG functional equivalence rooted in the coevolution of brain activations. They reveal hypnotizability-related sensory-cognitive information processing and of stronger functional equivalence between imagery and perception of the position of a body part in the subjects with high scores of hypnotizability. Moreover, our results provide insights of efficient versus expensive information processing between high and low type of hypnotizable subjects. Owing to the nature of TDA, this stronger functional equivalence is supported by non-local activation patterns, rather than by local regional activations, pointing to the need to characterize the changes in functional connectivity at the mesoscopic scale (Bassett and Sporns, 2017; Betzel et al., 2018). Spectral analysis of the studied sensory and imagined conditions had revealed imagery induced changes all over the brain but could not provide information regarding the relation between brain regions (Campioni et al., 2018). The direct comparison between spectral and topological analyses of actual rotation indicated that spectral analysis could detect the difference between head positions but not hypnotizability-related differences, which was revealed by TDA (Ibáñez-Marcelo et al., 2019). The relevance of topological approaches to this problem lies precisely in their capacity to provide quantitative measure of such observables (Petri et al., 2014; Sizemore et al., 2016).

Our findings are relevant in the field of hypnotizability, as they indicate a different embodiment of mental images supporting the proneness to ideomotor behavior, and in cognitive science, as the hypnotizability-related information processing can be a model to describe how different selves may emerge from neurophysiological assets. In this respect, the question *whether highs and lows live in the same world* (Carli et al., 2007), that is how they represent and reconstruct sensori-motor information, seems to be efficaciously addressed by TDA.

#### Author contributions statement

ELS designed the experiment, EIM and GP designed the analytical framework, LC and ELS conducted the experiment and preprocessed the data, EIM, GP and AP analysed the results. All authors wrote and reviewed the manuscript.

#### Competing financial interests

The authors declare no competing interest. The funders had no role in study design, data collection, and analysis, decision to publish, or preparation of the manuscript.

#### Acknowledgements

EIM and GP are supported by the ADnD project of Compagnia San Paolo. GP acknowledges partial support from Intesa Sanpaolo Innovation Center.

### Appendix A. Mathematical formulation of homology and persistent homology

We introduce some technical notions in the context of persistent homology: chain complex, boundary map and the formal definition of homology (Munkres, 2000; Hatcher, 2002).

The set of  $n$ -dimensional chains  $C_n(X)$  of a simplicial complex  $X$  is the formal sums of  $n$ -simplices. Formally written as,

$$C_n(X) = \{r_1\sigma_1 + r_2\sigma_2 + \dots + r_i\sigma_i \mid r_i \in \mathbb{Z}, \sigma_i \in X_n\}. \tag{A.1}$$

Then we can define a *boundary map*  $\partial_n$  between  $n$ -dimensional chains  $C_n(X)$  to  $(n - 1)$ -dimensional chains  $C_{n-1}(X)$  that corresponds to our intuitive notion of boundary.

$$\partial_n : C_n(X) \rightarrow C_{n-1}(X) \tag{A.2}$$

$$[v_1, \dots, v_n] \mapsto \sum_{i=0}^n (-1)^i [v_0, \dots, \widehat{v}_i, \dots, v_n] \tag{A.3}$$

where the hat denotes the omission of the vertex and this map satisfies  $\partial_n \partial_{n+1} = 0 \quad \forall n$ . For example, if we have a simplex of dimension 2 (a full triangle), it will be converted to its boundary, that is, three concatenated edges (simplices of dimension 1). The boundary of a simplex is the alternating sum of restrictions to its faces.

A simplicial complex  $X$  induces the *chain complex*,  $\dots \rightarrow C_{n+1} \rightarrow C_n \rightarrow C_{n-1} \rightarrow \dots$  through boundary maps  $\dots \partial_{n+2}, \partial_{n+1}, \partial_n, \partial_{n-1}, \dots$

The  $n$ -homology of this complex is defined by the quotient of two vector spaces, the kernel of the map  $\partial_n$  quotiented by the image of the boundary map one upper dimension,  $\partial_{n+1}$ ,

$$H_n(X) = \ker \partial_n / \text{im } \partial_{n+1}, \tag{A.4}$$

where  $n$  indicates the dimension of the generators in the homology group. We call the kernel  $\ker \partial_n$  the  $n$ th cycle module, denoted  $Z_n$ , and the image  $\text{im } \partial_n$  the  $n$ th boundary module, denoted  $B_n$ .

Formally, given a simplicial complex  $X$ , a filtration is a totally ordered set of subcomplexes  $X_i \subset X$ , that starts with the empty complex and ends with the complete complex, indexed by the nonnegative integers,

$$\emptyset = X_0 \subseteq X_1 \subseteq \dots \subseteq X_m = X \tag{A.5}$$

such that if  $i \leq j$  then  $X_i \subseteq X_j$ . The total ordering itself is called a filtration. The subcomplexes  $X_i$  are the analog of the sublevel sets in the Morse function setting (Milnor, 2016).

In order to define *persistent homology* (Edelsbrunner and Harer, 2008; Zomorodian and Carlsson, 2005), we use superscripts to denote the index in a filtration. The  $i$ th simplicial complex  $X_i$  in a filtration gives rise to its own chain complex  $(C_i^\bullet, \partial_i^\bullet)$  and the  $k$ th chain, cycle, boundary and homology modules are denoted by  $C_k^i, Z_k^i, B_k^i$  and  $H_k^i$ , respectively.

For a positive integer  $p$ , the  $p$ -persistent  $k$ th homology module of  $X_i$  is

$$H_k^{i,p} = Z_k^i / (B_k^{i+p} \cap Z_k^i) \tag{A.6}$$

The form of  $H_k^{i,p}$  should seem similar to the formula for  $H_k^i$ , except that instead of characterizing the  $k$ -cycles in  $X_i$  that do not come from a  $(k + 1)$ -chain in  $X_i$ , it characterizes the  $k$ -cycles in the  $X_i$  subcomplex that are not the boundary of any  $(k + 1)$ -chain from the larger complex  $X_{i+p}$ . Put another way,  $H_k^{i,p}$  characterizes the  $k$ -dimensional holes in  $X_{i+p}$  created by the subcomplex  $X_i$ . These holes exist for all complexes  $X_j$  in the filtration with index  $i \leq j \leq i + p$ .

### Appendix B. Tables

**Table B1**  
 $t$ -test results for the differences between  $\Omega(X, X)$  and  $\Omega(bX, bX)$  for *highs* and *lows* in Fig. 2.

Condition	$t$ -test $\Omega(X, X)$	p-value	$t$ -test $\Omega(bX, bX)$	p-value
k1	5.5	0.00058	4.3	6.9e-05
v1	4.2	3.7e-08	9.8	6.6e-14
rr	7.4	4.1e-12	8.6	6e-12
k2	9.1	7.2e-08	5.2	2.5e-06
v2	6.9	1.1e-07	8.7	3.9e-12

**Table B.2**  
t-test results for the differences between  $K_\sigma(X, bX)$  for *highs* and *lows* in Fig. 4.

Condition	t-test $K_\sigma(X, bX)$	p-value
k1	-3.63	0.0005
v1	-6.33	3.72e-8
rr	-8.70	4.11e-12
k2	-6.16	7.23e-8
v2	-6.05	1.10e-7

**Table B.3**  
t-test results on the mean value for different conditions in Fig. 5.

Condition	t-test	p-value
k1	22.75	4.83e-20
k2	27.00	4.19e-22
v1	24.86	4.22e-21
v2	19.60	2.85e-18
$\Delta k$	65.76	4.07e-33
$\Delta v$	19.42	3.64e-18

**Table B.4**  
t-test results on the mean value for different conditions in Fig. 6.

Condition	t-test	p-value
Highs (k1,k2)	46.4	1.4e-47
Highs (v1,v2)	22.	8.9e-30
Lows (k1,k2)	5.8	2.8e-07
Lows (v1,v2)	17.4	1.e-24

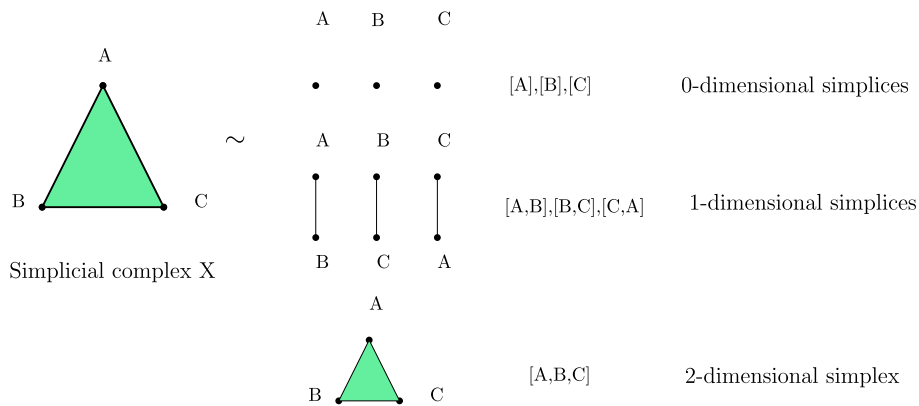


**Fig. B.7.** An example of simplicial complex,  $X$  and its pieces:  $X = \{[A], [B], [C], [A, B], [B, C], [C, A], [A, B, C]\}$ . In other words, a full triangle is composed by three 0-simplices (points), three 1-simplices (segments) and a 2-simplex (a full triangle).

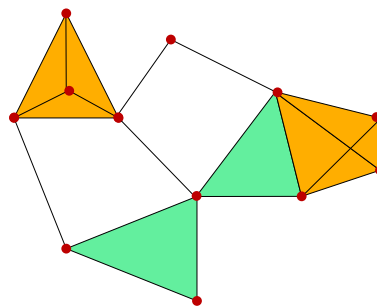


**Fig. B.8.** Clique complex of a network. Cliques in the network are mapped (*filled*) to simplices of the corresponding dimension in order to obtain a simplicial complex.

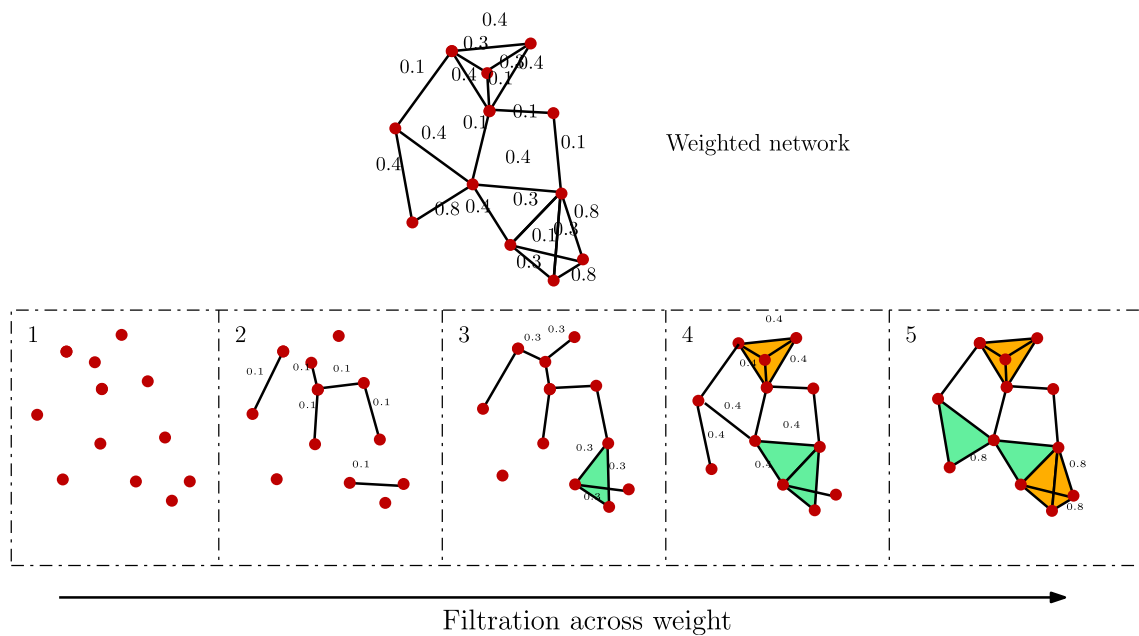


Fig. B.9. Clique complex filtration over weights of a weighted network.

### Persistent diagrams and similarity measure

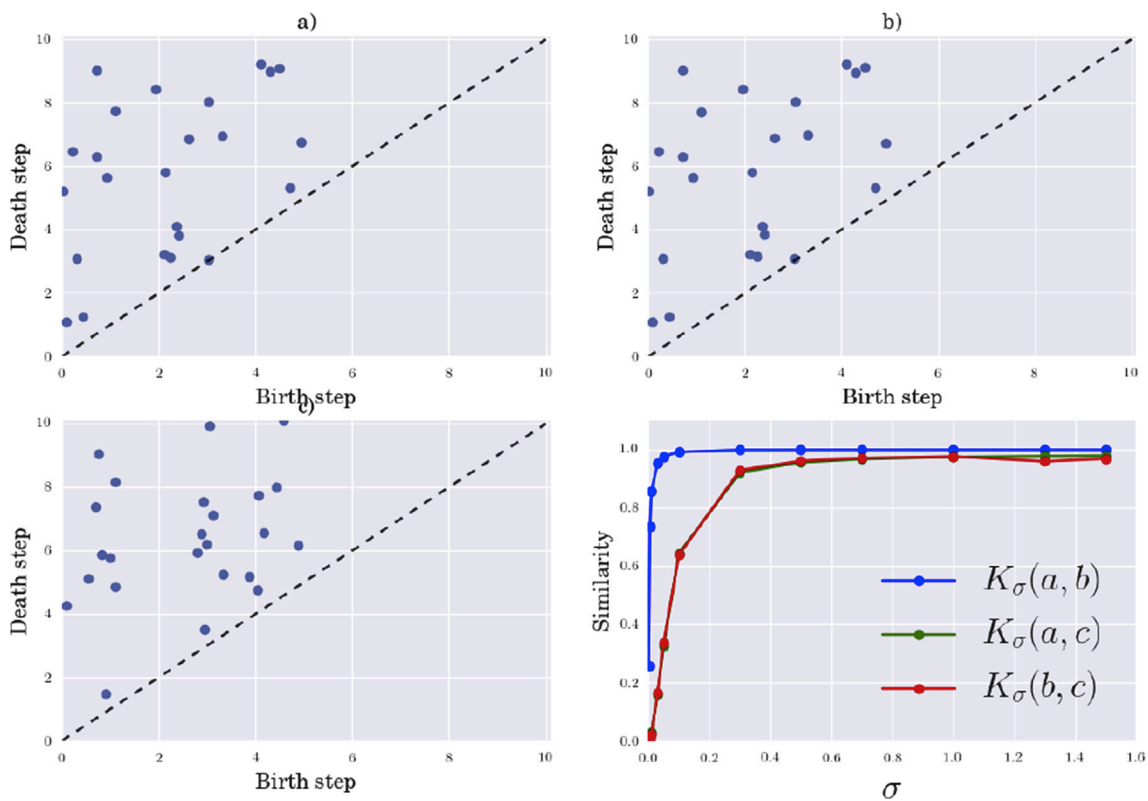
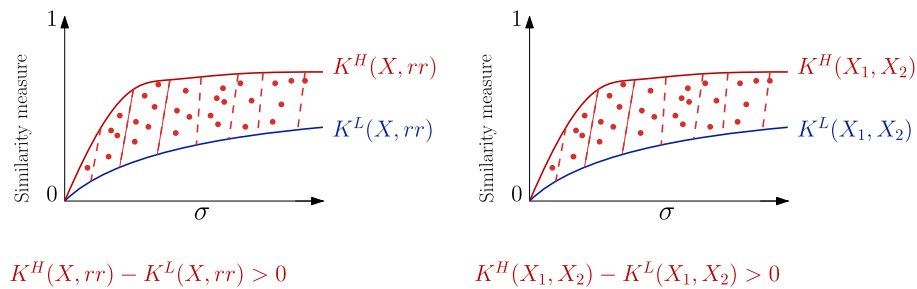
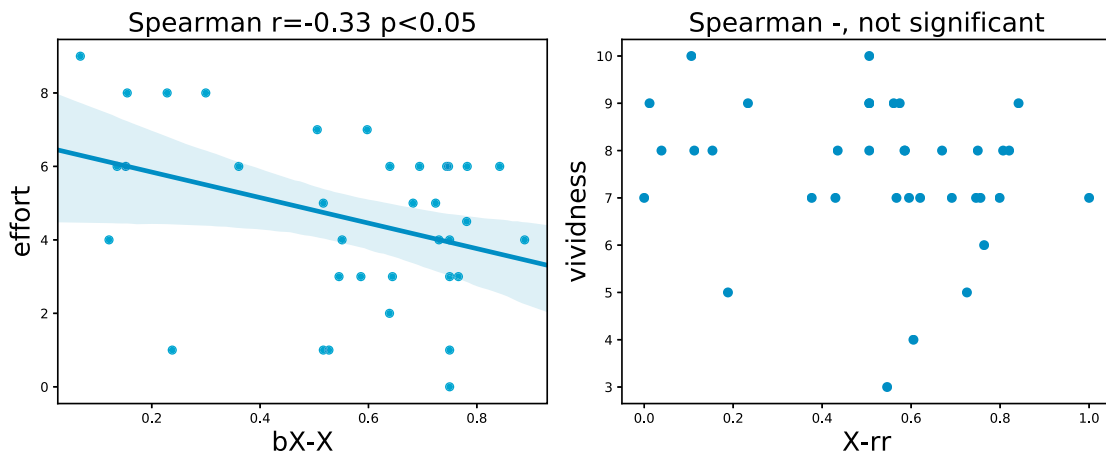


Fig. B.10. Examples of persistence diagrams in a), b) c) and similarity measure between them. Points further from the diagonal (dotted line) in persistent diagrams represent cycles with a larger persistence along filtration. Similarity between a) and b) is higher than similarity between a) and c) and b) and c),  $K_\sigma(a, c) \ll K_\sigma(a, b)$  and  $K_\sigma(b, c) \ll K_\sigma(a, b)$ .



**Fig. B.11. Difference between *highs* and *lows* of imagery tasks and real rotation across similarity curves obtained from persistence diagrams.** Left: Difference between *highs* and *lows* of imagery tasks alteration of topology relate the actual rotations ( $rr$ ). Positive results shows how *highs* are always topological nearer to the real rotation than *lows* for all imagery conditions. Right: Difference between *highs* and *lows* of imagery tasks alteration of topology before ( $k1,v1$ ) and after ( $k2,v2$ ) the actual rotation. Positive results show how *highs* both in kinesthetic and visual imaginations are always topological nearer to the real rotation or that real rotation does not inference in their imagination than *lows* for all imagery conditions.



**Fig. B.12. Individual correlations.** Aggregating all imagery tasks, we show the relation between the subjective values between effort and  $\Omega(bX, X)$  (left), and between vividness and  $\Omega(rr, X)$  (right). In the first case, as expected we recover a (significant,  $r = -0.33$ ,  $p < 0.05$ ) negative correlation between basal deviation and reported effort. For vividness at the subjective level our results are inconclusive as we do not find significant correlations.

## References

- Anuar, N., Williams, S.E., Cumming, J., 2017. Do the physical and environment pettle elements predict sport imagery ability? *Eur. J. Sport Sci.* 17 (10), 1319–1327.
- Arai, M., Brandt, V., Dabaghian, Y., 2014. The effects of theta precession on spatial learning and simplicial complex dynamics in a topological model of the hippocampal spatial map. *PLoS Comput. Biol.* 10 (6), e1003651.
- Bartolomeo, P., 2002. The relationship between visual perception and visual mental imagery: a reappraisal of the neuropsychological evidence. *Cortex* 38 (3), 357–378.
- Bassett, D.S., Sporns, O., 2017. Network neuroscience. *Nat. Neurosci.* 20 (3), 353.
- Bell, P.T., Shine, J.M., 2016. Subcortical contributions to large-scale network communication. *Neurosci. Biobehav. Rev.* 71, 313–322.
- Bensafi, M., Pouliot, S., Sobel, N., 2005. Odorant-specific patterns of sniffing during imagery distinguish “bad” and “good” olfactory imagers. *Chem. Senses* 30 (6), 521–529.
- Betz, R.F., Medaglia, J.D., Bassett, D.S., 2018. Diversity of meso-scale architecture in human and non-human connectomes. *Nat. Commun.* 9 (1), 346.
- Bocci, T., Barloscio, D., Parenti, L., Sartucci, F., Carli, G., Santarcangelo, E.L., 2016. High hypnotizability impairs the cerebellar control of pain. *The Cerebellum* 16(1):55–61.
- Bowers, K.S., 1992. Imagination and dissociation in hypnotic responding. *Int. J. Clin. Exp. Hypn.* 40 (4), 253–275.
- Caligiore, Daniele, et al., 2017. Action observation and motor imagery for rehabilitation in Parkinson’s disease: A systematic review and an integrative hypothesis. *Neurosci. Biobehav. Rev.* 72, 210–222.
- Campioni, L., Banfi, T., Santarcangelo, E.L., 2018. Hypnotizability influences the cortical representation of visually and kinaesthetically imagined head position. *Brain Cogn.* 123, 120–125.
- Carli, G., Rendo, C., Sebastiani, L., Santarcangelo, E.L., 2006. Suggestions of altered balance: possible equivalence of imagery and perception. *Int. J. Clin. Exp. Hypn.* 54 (2), 206–223.

- Carli, G., Cavallaro, F., Rendo, C., Santarcangelo, E., 2007. Imagery of different sensory modalities: hypnotizability and body sway. *Exp. Brain Res.* 179 (2), 147–154.
- Castellani, E., Sebastiani, L., 2008. Manipulation of attention in highly and low hypnotizable individuals: a study on verbal priming. *Arch. Ital. Biol.* 146 (1), 21.
- Castellani, E., D’Alessandro, L., Sebastiani, L., 2007. Hypnotizability and spatial attentional functions. *Arch. Ital. Biol.* 145 (1), 23–37.
- Cavallaro, F.I., Cacace, I., Del Testa, M., Andre, P., Carli, G., De Pascalis, V., Rocchi, R., Santarcangelo, E.L., 2010. Hypnotizability-related eeg alpha and theta activities during visual and somesthetic imageries. *Neurosci. Lett.* 470 (1), 13–18.
- Cheron, Petit, G., Cheron, J., Leroy, A., Cebolla, A., Cevallos, C., Petieau, M., Hoellinger, T., Zarka, D., Clarinval, A.M., et al., 2016. Brain oscillations in sport: toward eeg biomarkers of performance. *Front. Psychol.* 7, 246.
- Choi, H., Kim, Y.K., Kang, H., Lee, H., Im, H.J., Kim, E.E., Chung, J.K., Lee, D.S., et al., 2014. Abnormal metabolic connectivity in the pilocarpine-induced epilepsy rat model: a multiscale network analysis based on persistent homology. *Neuroimage* 99, 226–236.
- Chung, M.K., Bubenik, P., Kim, P.T., 2009. Persistence diagrams of cortical surface data. In: *International Conference on Information Processing in Medical Imaging*. Springer, pp. 386–397.
- Chung, M.K., Villalta-Gil, V., Lee, H., Rathouz, P.J., Lahey, B.B., Zald, D.H., 2017. Exact topological inference for paired brain networks via persistent homology. In: *International Conference on Information Processing in Medical Imaging*. Springer, pp. 299–310.
- Cojan, Y., Piguet, C., Vuilleumier, P., 2015. What makes your brain suggestible? hypnotizability is associated with differential brain activity during attention outside hypnosis. *Neuroimage* 117, 367–374.
- Crawford, H.J., 1994. Brain dynamics and hypnosis: attentional and disattentional processes. *Int. J. Clin. Exp. Hypn.* 42 (3), 204–232.
- Cremades, J.G., Pease, D.G., 2007. Concurrent validity and reliability of lower and upper alpha activities as measures of visual and kinesthetic imagery ability. *Int. J. Sport Exerc. Psychol.* 5 (2), 187–202.

- David, D., Brown, R.J., 2002. Suggestibility and negative priming: two replication studies. *Int. J. Clin. Exp. Hypn.* 50 (3), 215–228.
- de Borst, A.W., de Gelder, B., 2016. fmri-based multivariate pattern analyses reveal imagery modality and imagery content specific representations in primary somatosensory, motor and auditory cortices. *Cerebr. Cortex* 1–15.
- Del Percio, C., Infarinato, F., Iacoboni, M., Marzano, N., Soricelli, A., Aschieri, P., Eusebi, F., Babiloni, C., 2010. Movement-related desynchronization of alpha rhythms is lower in athletes than non-athletes: a high-resolution eeg study. *Clin. Neurophysiol.* 121 (4), 482–491.
- Di Gruttola, F., Orsini, P., Carboncini, M.C., Rossi, B., Santarcangelo, E.L., 2014. Revisiting the association between hypnotisability and blink rate. *Exp. Brain Res.* 232 (12), 3763–3769.
- Edelsbrunner, H., Harer, J., 2008. Persistent homology—a survey. *Contemp. Math.* 453, 257–282.
- Elkins, G.R., Barabasz, A.F., Council, J.R., Spiegel, D., 2015. Advancing research and practice: the revised apa division 30 definition of hypnosis. *Int. J. Clin. Exp. Hypn.* 63 (1), 1–9.
- Elton, A., Gao, W., 2015. Task-related modulation of functional connectivity variability and its behavioral correlations. *Hum. Brain Mapp.* 36 (8), 3260–3272.
- Finke, R.A., 1979. The functional equivalence of mental images and errors of movement. *Cogn. Psychol.* 11 (2), 235–264.
- Frank, C., Schack, T., 2017. The representation of motor (inter) action, states of action, and learning: three perspectives on motor learning by way of imagery and execution. *Front. Psychol.* 8.
- Ganea, N., Longo, M.R., 2017. Projecting the self outside the body: body representations underlying proprioceptive imagery. *Cognition* 162, 41–47.
- Ganis, G., Thompson, W.L., Kosslyn, S.M., 2004. Brain areas underlying visual mental imagery and visual perception: an fmri study. *Cogn. Brain Res.* 20 (2), 226–241.
- Ghrist, R., 2008. Barcodes: the persistent topology of data. *Bull. Am. Math. Soc.* 45 (1), 61–75.
- Giusti, C., Pastalkova, E., Curto, C., Itskov, V., 2015. Clique topology reveals intrinsic geometric structure in neural correlations. *Proc. Natl. Acad. Sci.* 112 (44), 13455–13460.
- Gruzelier, J.H., 2006. Frontal functions, connectivity and neural efficiency underpinning hypnosis and hypnotic susceptibility. *Contemp. Hypn.* 23 (1), 15–32.
- Guerraz, M., Day, B.L., 2005. Expectation and the vestibular control of balance. *J. Cogn. Neurosci.* 17 (3), 463–469.
- Guillot, A., Collet, C., Nguyen, V.A., Malouin, F., Richards, C., Doyon, J., 2008. Functional neuroanatomical networks associated with expertise in motor imagery. *Neuroimage* 41 (4), 1471–1483.
- Halpern, A.R., Zatorre, R.J., 1999. When that tune runs through your head: a pet investigation of auditory imagery for familiar melodies. *Cerebr. Cortex* 9 (7), 697–704.
- Hatcher, A., 2002. *Algebraic Topology*. Cambridge University Press.
- Hatfield, B.D., Haufler, A.J., Hung, T.M., Spalding, T.W., 2004. Electroencephalographic studies of skilled psychomotor performance. *J. Clin. Neurophysiol.* 21 (3), 144–156.
- Hétu, S., Grégoire, M., Saimpont, A., Coll, M.P., Eugène, F., Michon, P.E., Jackson, P.L., 2013. The neural network of motor imagery: an ale meta-analysis. *Neurosci. Biobehav. Rev.* 37 (5), 930–949.
- Hilgard, E.R., 1991. *A Neodissociation Interpretation of Hypnosis*. Guilford Press.
- Hilgard, E.R., Hilgard, J.R., 2013. *Hypnosis in the Relief of Pain*. Routledge.
- Hilton, P.J., Wylie, S., 1967. *Homology Theory: an Introduction to Algebraic Topology*. CUP Archive.
- Ibáñez-Marcelo, E., Campioni, L., Manzoni, D., Santarcangelo, E.L., Petri, G., 2019. Spectral and topological analysis of the cortical representation of the head position: does hypnotizability matter? *Brain & Behaviour* 9, e01277. <https://doi.org/10.1002/brb3.1277>.
- James, W., 1890. *The principles of Psychology* 2.
- Jeannerod, M., 1995. Mental imagery in the motor context. *Neuropsychologia* 33 (11), 1419–1432.
- Kasos, E., Kasos, K., Pusztai, F., Polyák, Á., Kovács, K.J., Varga, K., 2018. Changes in oxytocin and cortisol in active-alert hypnosis: hormonal changes benefiting low hypnotizable participants. *Int. J. Clin. Exp. Hypn.* 66 (4), 404–427.
- Khalid, A., Kim, B.S., Am Seo, B., Lee, S.T., Jung, K.H., Chu, K., Lee, S.K., Jeon, D., 2016. Gamma oscillation in functional brain networks is involved in the spontaneous remission of depressive behavior induced by chronic restraint stress in mice. *BMC Neurosci.* 17 (1), 4.
- Kilintari, M., Narayana, S., Babajani-Feremi, A., Rezaie, R., Papanicolaou, A.C., 2016. Brain activation profiles during kinesthetic and visual imagery: an fmri study. *Brain Res.* 1646, 249–261.
- Kim, H., Hahm, J., Lee, H., Kang, E., Kang, H., Lee, D.S., 2015. Brain networks engaged in audiovisual integration during speech perception revealed by persistent homology-based network filtration. *Brain Connect.* 5 (4), 245–258.
- Kirsch, I., 2018. Response expectancy and the placebo effect. In: *International Review of Neurobiology*, vol 138. Elsevier, pp. 81–93.
- Kosslyn, S.M., Thompson, W.L., Klm, L.J., Alpert, N.M., 1995. Topographical representations of mental images in primary visual cortex. *Nature* 378 (6556), 496.
- Kosslyn, S.M., Thompson, W.L., Ganis, G., 2006. *The Case for Mental Imagery*. Oxford University Press.
- Landry, M., Lifshitz, M., Raz, A., 2017. Brain correlates of hypnosis: a systematic review and meta-analytic exploration. *Neurosci. Biobehav. Rev.* 81, 75–98.
- Lebon, F., Byblow, W.D., Collet, C., Guillot, A., Stinear, C.M., 2012. The modulation of motor cortex excitability during motor imagery depends on imagery quality. *Eur. J. Neurosci.* 35 (2), 323–331.
- Lee, S., Kang, H., Chung, M.K., Kim, B.N., Lee, D.S., 2012. Persistent brain network homology from the perspective of dendrogram. *IEEE Trans. Med. Imaging* 31 (12), 2267–2277.
- Liang, H., Wang, H., 2017. Structure-function network mapping and its assessment via persistent homology. *PLoS Comput. Biol.* 13 (1), e1005325.
- Lima, C.F., Lavan, N., Evans, S., Agnew, Z., Halpern, A.R., Shanmugalingam, P., Meekings, S., Boebinger, D., Ostarek, M., McGittigan, C., et al., 2015. Feel the noise: relating individual differences in auditory imagery to the structure and function of sensorimotor systems. *Cerebr. Cortex* 25 (11), 4638–4650.
- Lord, L.D., Expert, P., Fernandes, H.M., Petri, G., Van Hartevelt, T.J., Vaccarino, F., Deco, G., Turkheimer, F., Kringelbach, M.L., 2016. Insights into brain architectures from the homological scaffolds of functional connectivity networks. *Front. Syst. Neurosci.* 10.
- Lund, S., Broberg, C., 1983. Effects of different head positions on postural sway in man induced by a reproducible vestibular error signal. *Acta Physiol.* 117 (2), 307–309.
- Lynn, S.J., 1997. Automaticity and hypnosis: a sociocognitive account. *Int. J. Clin. Exp. Hypn.* 45 (3), 239–250.
- Lynn, S.J., Green, J.P., 2011. The sociocognitive and dissociation theories of hypnosis: toward a rapprochement. *Int. J. Clin. Exp. Hypn.* 59 (3), 277–293.
- Madeo, D., Castellani, E., Santarcangelo, E.L., Mocenni, C., 2013. Hypnotic assessment based on the recurrence quantification analysis of eeg recorded in the ordinary state of consciousness. *Brain Cogn.* 83 (2), 227–233.
- Madeo, D., Castellani, E., Mocenni, C., Santarcangelo, E.L., 2015. Pain perception and eeg dynamics: does hypnotizability account for the efficacy of the suggestions of analgesia? *Physiol. Behav.* 145, 57–63.
- Marks, D.F., Isaac, A.R., 1995. Topographical distribution of eeg activity accompanying visual and motor imagery in vivid and non-vivid imagers. *Br. J. Psychol.* 86 (2), 271–282.
- Menzocchi, M., Mecacci, G., Zeppi, A., Carli, G., Santarcangelo, E.L., 2015. Hypnotizability and performance on a prism adaptation test. *The Cerebellum* 14 (6), 699–706.
- Meulen, M., Allali, G., Rieger, S.W., Assal, F., Vuilleumier, P., 2014. The influence of individual motor imagery ability on cerebral recruitment during gait imagery. *Hum. Brain Mapp.* 35 (2), 455–470.
- Meyer, E.C., Lynn, S.J., 2011. Responding to hypnotic and nonhypnotic suggestions: performance standards, imaginative suggestibility, and response expectancies. *Int. J. Clin. Exp. Hypn.* 59 (3), 327–349.
- Milnor, J., 2016. In: *Morse Theory*. (AM-51), vol 51. Princeton university press.
- Mizuguchi, N., Nakamura, M., Kanosue, K., 2017. Task-dependent engagements of the primary visual cortex during kinesthetic and visual motor imagery. *Neurosci. Lett.* 636, 108–112.
- Munkres, J.R., 2000. *Topology*. Prentice Hall.
- Oldfield, R.C., 1971. The assessment and analysis of handedness: the edinburgh inventory. *Neuropsychologia* 9 (1), 97–113.
- Papalia, E., Manzoni, D., Santarcangelo, E.L., 2014. Stabilizing posture through imagery. *Int. J. Clin. Exp. Hypn.* 62 (3), 292–309.
- Patania, A., Vaccarino, F., Petri, G., 2017. Topological analysis of data. *EPJ Data Sci.* 6 (1), 7.
- Pekala, R.J., Baglio, F., Cabinio, M., Lipari, S., Baglio, G., Mendozzi, L., Cecconi, P., Pugnelli, L., Sciaky, R., 2017. Hypnotism as a function of trance state effects, expectancy, and suggestibility: an Italian replication. *Int. J. Clin. Exp. Hypn.* 65 (2), 210–240.
- Petri, G., Scolamiero, M., Donato, I., Vaccarino, F., 2013. Topological strata of weighted complex networks. *PLoS One* 8 (6), e66506.
- Petri, G., Expert, P., Turkheimer, F., Carhart-Harris, R., Nutt, D., Hellyer, P.J., Vaccarino, F., 2014. Homological scaffolds of brain functional networks. *J. R. Soc. Interface* 11 (101), 20140873.
- Picerni, E., Santarcangelo, E., Laricchiuta, D., Cutuli, D., Petrosini, L., Spalletta, G., Piras, F., 2018. Cerebellar structural variations in subjects with different hypnotizability. *The Cerebellum* 1–10.
- Prete, G., Marzoli, D., Brancucci, A., Tommasi, L., 2016. Hearing it right: evidence of hemispheric lateralization in auditory imagery. *Hear. Res.* 332, 80–86.
- Rakusa, M., Busan, P., Battaglini, P.P., Zidar, J., 2017. Separating the idea from the action: a sloretta study. *Brain Topogr.* 1–14.
- Reimann, M.W., Nolte, M., Scolamiero, M., Turner, K., Perin, R., Chindemi, G., Dlotko, P., Levi, R., Hess, K., Markram, H., 2017. Cliques of neurons bound into cavities provide a missing link between structure and function. *Front. Comput. Neurosci.* 11, 48.
- Reininghaus, J., Huber, S., Bauer, U., Kwitt, R., 2015. A stable multi-scale kernel for topological machine learning. In: *Proceedings of the IEEE Conference on Computer Vision and Pattern Recognition*, pp. 4741–4748.
- Reynolds, R.F., 2010. The effect of voluntary sway control on the early and late components of the vestibular-evoked postural response. *Exp. Brain Res.* 201 (2), 133–139.
- Ridderinkhof, K.R., Brass, M., 2015. How kinesthetic motor imagery works: a predictive-processing theory of visualization in sports and motor expertise. *J. Physiol. Paris* 109 (1), 53–63.
- Rodionov, V., Zislin, J., Elidan, J., 2004. Imagination of body rotation can induce eye movements. *Acta Otolaryngol.* 124 (6), 684–689.
- Rubinov, M., Sporns, O., 2010. Complex network measures of brain connectivity: uses and interpretations. *Neuroimage* 52 (3), 1059–1069.
- Ruehle, B.L., Zamansky, H.S., 1997. The experience of effortlessness in hypnosis: perceived or real? *Int. J. Clin. Exp. Hypn.* 45 (2), 144–157.
- Santarcangelo, E.L., 2014. New views of hypnotizability. *Front. Behav. Neurosci.* 8.
- Santarcangelo, E., Cavallaro, E., Mazzoleni, S., Marano, E., Ghelarducci, B., Dario, P., Micera, S., Sebastiani, L., 2005. Kinematic strategies for lowering of upper limbs

- during suggestions of heaviness: a real-simulator design. *Exp. Brain Res.* 162 (1), 35–45.
- Santarcangelo, E.L., Scattina, E., Carli, G., Ghelarducci, B., Orsini, P., Manzoni, D., 2010. Can imagery become reality? *Exp. Brain Res.* 206 (3), 329–335.
- Scattina, E., Huber, A., Menzocchi, M., Paoletti, G., Carli, G., Manzoni, G., Santarcangelo, E.L., 2012. Postural effects of imagined leg pain as a function of hypnotizability. *Exp. Brain Res.* 216 (3), 341–348.
- Schmidt, T.T., Ostwald, D., Blankenburg, F., 2014. Imaging tactile imagery: changes in brain connectivity support perceptual grounding of mental images in primary sensory cortices. *Neuroimage* 98, 216–224.
- Schultz, D.H., Cole, M.W., 2016. Higher intelligence is associated with less task-related brain network reconfiguration. *J. Neurosci.* 36 (33), 8551–8561.
- Sheehan, P.W., McConkey, K.M., 1982. Hypnosis and Experience. The exploration of phe.
- Sheldon, S., El-Asmar, N., 2017. The cognitive tools that support mentally constructing event and scene representations. *Memory* 1–11.
- Shin, L.M., Kosslyn, S.M., McNally, R.J., Alpert, N.M., Thompson, W.L., Rauch, S.L., Macklin, M.L., Pitman, R.K., 1997. Visual imagery and perception in posttraumatic stress disorder: a positron emission tomographic investigation. *Arch. Gen. Psychiatr.* 54 (3), 233–241.
- Shine, J.M., Bissett, P.G., Bell, P.T., Koyejo, O., Balsters, J.H., Gorgolewski, K.J., Moodie, C.A., Poldrack, R.A., 2016. The dynamics of functional brain networks: integrated network states during cognitive task performance. *Neuron* 92 (2), 544–554.
- Sizemore, A., Giusti, C., Bassett, D.S., 2016. Classification of weighted networks through mesoscale homological features. *J. Complex Netw.* 5 (2), 245–273.
- Slotnick, S.D., Thompson, W.L., Kosslyn, S.M., 2012. Visual memory and visual mental imagery recruit common control and sensory regions of the brain. *Cogn. Neurosci.* 3 (1), 14–20.
- Smith, M.E., McEvoy, L.K., Gevins, A., 1999. Neurophysiological indices of strategy development and skill acquisition. *Cogn. Brain Res.* 7 (3), 389–404.
- Spanos, N.P., 1986. Hypnosis and the modification of hypnotic susceptibility: a social psychological perspective. What is hypnosis 85–120.
- Spearman, C., 1904. The proof and measurement of association between two things. *Am. J. Psychol.* 15 (1), 72–101.
- Sporns, O., 2013. Network attributes for segregation and integration in the human brain. *Curr. Opin. Neurobiol.* 23 (2), 162–171.
- Spreemann, G., Dunn, B., Botnan, M.B., Baas, N.A., 2015. Using Persistent Homology to Reveal Hidden Information in Neural Data arXiv preprint arXiv:151006629.
- Stolz, B.J., Harrington, H.A., Porter, M.A., 2017. Persistent homology of time-dependent functional networks constructed from coupled time series. *Chaos: Interdiscip. J. Nonlinear Sci.* 27 (4), 047410.
- Szpunar, K.K., Watson, J.M., McDermott, K.B., 2007. Neural substrates of envisioning the future. *Proc. Natl. Acad. Sci.* 104 (2), 642–647.
- Terhune, D.B., Cardeña, E., 2015. Heterogeneity in high hypnotic suggestibility and the neurophysiology of hypnosis. *Neurophysiologie Clinique/Clin. Neurophysiol.* 45 (2), 177–178.
- Tong, Y., Pandy Jr., J.T., Li, W.A., Du, H., Zhang, T., Geng, X., Ding, Y., 2017. Motor imagery-based rehabilitation: potential neural correlates and clinical application for functional recovery of motor deficits after stroke. *Aging Dis.* 8 (3), 364.
- Wang, Y., Ombao, H., Chung, M.K., 2015. Topological seizure origin detection in electroencephalographic signals. In: 2015 IEEE 12th International Symposium on Biomedical Imaging (ISBI). IEEE, pp. 351–354.
- Wang, Y., Ombao, H., Chung, M.K., 2018. Topological data analysis of single-trial electroencephalographic signals. *Ann. Appl. Stat.* 12 (3), 1506.
- Weitzenhoffer, A.M., Hilgard, E.R., 1962. In: Stanford Hypnotic Susceptibility Scale, Form C, vol 27. Consulting Psychologists Press, Palo Alto, CA.
- Yoo, J., Kim, E.Y., Ahn, Y.M., Ye, J.C., 2016. Topological persistence vineyard for dynamic functional brain connectivity during resting and gaming stages. *J. Neurosci. Methods* 267, 1–13.
- Zomorodian, A., Carlsson, G., 2005. Computing persistent homology. *Discrete Comput. Geom.* 33 (2), 249–274.